applied sciences

MDPI

Article

Experimental Study on Post-Grouting Pile Vertical Bearing Performance Considering Different Grouting Methods and Parameters in Cohesive Soil

Jiaqi Zhang [1], Chunfeng Zhao [1,2,*] and Yue Wu [3]

[1] Department of Geotechnical Engineering, Tongji University, Shanghai 200092, China; zjq@tongji.edu.cn
[2] Key Laboratory of Geotechnical and Underground Engineering of Ministry of Education, Tongji University, Shanghai 200092, China
[3] School of Civil Engineering, Chongqing Jiaotong University, Chongqing 400074, China; cqjtuwy@cqjtu.edu.cn
* Correspondence: tjzhchf@163.com

Featured Application: This study provides valuable insights into the behavior and performance of grouted piles, contributing to the optimization of grouting methods and parameters for enhancing pile-bearing capacity in cast-in-place bored pile engineering projects.

Abstract: The selection of grouting methods and parameters significantly affects the improvement in the pile-bearing capacity of cast-in-place bored piles. This study proposes a comprehensive set of test methods for constructing model piles, performing grouting at the pile tip and pile side. A series of single-pile grouting and static load tests were conducted using these test methods. The results reveal that pile-side grouting is more effective in controlling pile settlement compared to tip grouting. Furthermore, tip-side-combined grouting exhibits superior reinforcement effects compared to the other two grouting methods. After grouting, a grout bubble is formed at the outlet, consisting of a compact diffusion zone internally and a split diffusion zone externally. Additionally, a vertical diffusion of grout occurs along the pile body, establishing a lateral friction resistance enhancement region. Within this region, the lateral friction resistance of the pile shows a negative correlation with the distance from the grouting outlet. The test results emphasize the significance of grouting volume and its impact on the bearing capacity, settlement control, lateral friction resistance, and grout bubble size in grouted piles, while the influence of variation in grouting pressure in a small range on bearing characteristics is not significantly apparent.

Keywords: cast-in-place pile; post-grouting; grouting volume; grouting pressure; grout diffusion range

check for updates

Citation: Zhang, J.; Zhao, C.; Wu, Y. Experimental Study on Post-Grouting Pile Vertical Bearing Performance Considering Different Grouting Methods and Parameters in Cohesive Soil. *Appl. Sci.* **2023**, *13*, 12175. https://doi.org/10.3390/app132212175

Academic Editor: Tiago Miranda

Received: 11 October 2023
Revised: 2 November 2023
Accepted: 3 November 2023
Published: 9 November 2023

Copyright: © 2023 by the authors. Licensee MDPI, Basel, Switzerland. This article is an open access article distributed under the terms and conditions of the Creative Commons Attribution (CC BY) license (https://creativecommons.org/licenses/by/4.0/).

1. Introduction

Cast-in-place bored pile foundations are extensively utilized in the construction of high-rise buildings, highways, and large-span bridges due to their numerous advantages, including simplified construction process, minimal noise, adaptability to different soil layers, flexible selection of length–diameter ratio, and high load-bearing capacity [1–4]. However, during construction, sedimentation on the pile bottom and the formation of slurry cake can have adverse effects on the bearing capacity of bored piles. To address these challenges, post-grouting has emerged as a common practice in practical engineering [5–7].

Post-grouting technology involves injecting cement-based grout as the primary agent into the pile tip or adjacent soil through grouting pipelines, once the concrete forming the pile body reaches a specific level of strength. This process, known as pile post-grouting, effectively pressurizes the grout, thereby improving the overall performance of the piles [8–10]. Post-grouting methods generally encompass three forms: tip grouting, side grouting, and tip-side combined grouting. Tip grouting significantly enhances the

mechanical properties of the weak layer at the pile bottom, mitigates the effects of sedimentation, and improves the pile-tip bearing capacity. Side grouting primarily fills the weak surface between the pile and soil, enhancing the shear performance of the surrounding soil and increasing the lateral friction resistance of the piles. Combined grouting exhibits characteristics of both methods [11,12].

Since its initial application to bridge pier pile foundations in the last century [13], post-grouting technology has been subject to extensive research in the field of pile foundations. These studies have focused on several key aspects: (1) grouting technology research, which constituted a significant research direction in the early stages. This line of inquiry encompassed investigations into various aspects, such as different grouting positions, grouting devices, and grouting methods [14–16]. (2) Field test research, which is the most prevalent method employed to study post-grouting technology. Field tests provide accurate data on the bearing characteristics of piles and the physical and mechanical properties of soil layers. Notably, Gouvenot and Gabiax's post-grouting tests in sandy and cohesive soil [17] demonstrated that post-grouting can increase the tip-bearing capacity of large-diameter bored piles threefold. Bustamante's pile side grouting test [14] revealed that grouting can ameliorate soil stress relaxation resulting from drilling, leading to a 2.5-fold increase in side friction resistance. Hu et al.'s field tests on three large-diameter super-long rock-socketed piles [5] demonstrated that combined grouting can enhance side resistance, tip resistance, and ultimate bearing capacity by 34–179%, 111–180%, and 113–138%, respectively. (3) Model test research, offering greater flexibility in experimental design and lower implementation costs compared to field tests. Model tests are typically conducted to investigate the bearing characteristics of grouted piles in specific soil layers or validate new grouting methods [2,6,7,9,18,19]. (4) Numerical simulation research, which is primarily employed to study complex real-world conditions and verify test results. However, due to the challenges associated with accurately simulating the grouting effect, this approach is relatively less utilized [18,20,21]. (5) Grout diffusion research, encompassing investigations into the rheological and diffusion characteristics of cement grout, as well as the diffusion range in post-grouting [22–29]. (6) Theoretical research, primarily involving the establishment of models to analyze the reinforcement mechanism of grouting and the load transfer mechanism of grouted piles [30–33].

The existing body of research has significantly advanced our understanding of the impact of post-grouting on pile-bearing capacity enhancement, as well as the improvement of tip and lateral resistance. However, several deficiencies remain: (1) most of the existing research primarily focuses on a single grouting form, neglecting to explore the differential effects and efficiency of various grouting forms. This limitation hinders the flexible selection of grouting methods in engineering applications. (2) There is a lack of systematic studies investigating the influence of grouting volume and pressure on the reinforcement range and effect. Consequently, accurate calculation and prediction of pile-bearing capacity are compromised, leading to an overreliance on increased safety factors in engineering design, which results in unnecessary economic waste. (3) Current model test studies often overlook the unloading effect of soil mass during the drilling process of cast-in-place piles. This oversight creates a gap between the analysis results and actual engineering scenarios [34]. Therefore, in order to address the aforementioned deficiencies and enhance the application efficiency of post-grouting techniques in pile foundations, the author aims to investigate the variations among various grouting methods and systematically study the influence of grout volume and pressure, as well as consider the soil unloading effect during the drilling process. In this manner, the accuracy and efficiency of pile reinforcement and bearing capacity prediction can be significantly improved. This, in turn, will contribute to more cost-effective and optimized engineering practices.

Building upon the aforementioned analysis, this research proposes a novel model pile construction method capable of achieving both tip, side, and tip-side combined grouting. The study further conducts model tests to evaluate the vertical bearing capacity of individual piles, considering different grouting volumes and grouting pressures. Through

an analysis of the load-displacement relationship at the pile top, as well as the lateral friction resistance and tip resistance, the efficiency of various grouting forms in enhancing pile-bearing capacity and the reinforcement effects under different grouting parameters are thoroughly examined. Following the completion of the tests, the excavated piles are subjected to an analysis of the grouting body to investigate the diffusion range and diffusion mechanism of the grout. This comprehensive examination contributes valuable insights for both the calculation and construction of grouted piles, providing a reliable reference for future engineering applications.

2. Vertical Static Load Model Experiment Scheme

2.1. Test Site and Model Soil

The experimental setup employed in this investigation is a substantial testing chamber located at the Key Laboratory of Geotechnical and Underground Engineering of the Ministry of Education at Tongji University [2,33]. The chamber, as depicted in Figure 1, is composed of reinforced concrete and measures 3.0 × 2.1 × 3.0 m, with a wall thickness of 0.3 m. To create the model soil, clay material obtained from a stratum in Shanghai Province, China, underwent processes of gravel extraction and large particle crushing. The resulting soil was then arranged into uniform layers of 0.2 m thickness and compacted within the testing chamber. The specific parameters measured during the experiment are tabulated in Table 1.



Figure 1. Test chamber.

Table 1. Soil parameters of the model test.

Moisture Content (%)	Liquid Limit (%)	Plastic Limit (%)	Cohesion (kPa)	Internal Friction Angle (°)	Density ($kg \cdot m^{-3}$)
23.4	36	21	16.2	16.7	1870

2.2. Preparation of Model Piles

In this study, a model pile was utilized, with a buried depth of 1.8 m and a length of 1.9 m. Pile diameter is 46 mm. The pile consisted of three main components, namely, an internal pile core, a cement mortar pile body, and grouting pipes, as depicted in Figure 2. The dimensions of the pile core measure 25 × 15 mm, which was constructed using two

L-shaped angle aluminum pieces spliced together to simulate steel reinforcement. Strain gauges were symmetrically positioned along the long edge of the pile core at intervals of 0.25 m to monitor the internal forces experienced during the loading process. Following the creation of each pile core, the wire was carefully extracted. Subsequently, the pile cores were securely wrapped with gauze and affixed in place, after which they were coated with epoxy resin to undergo waterproofing treatment. The completed pile core is shown in Figure 3a.

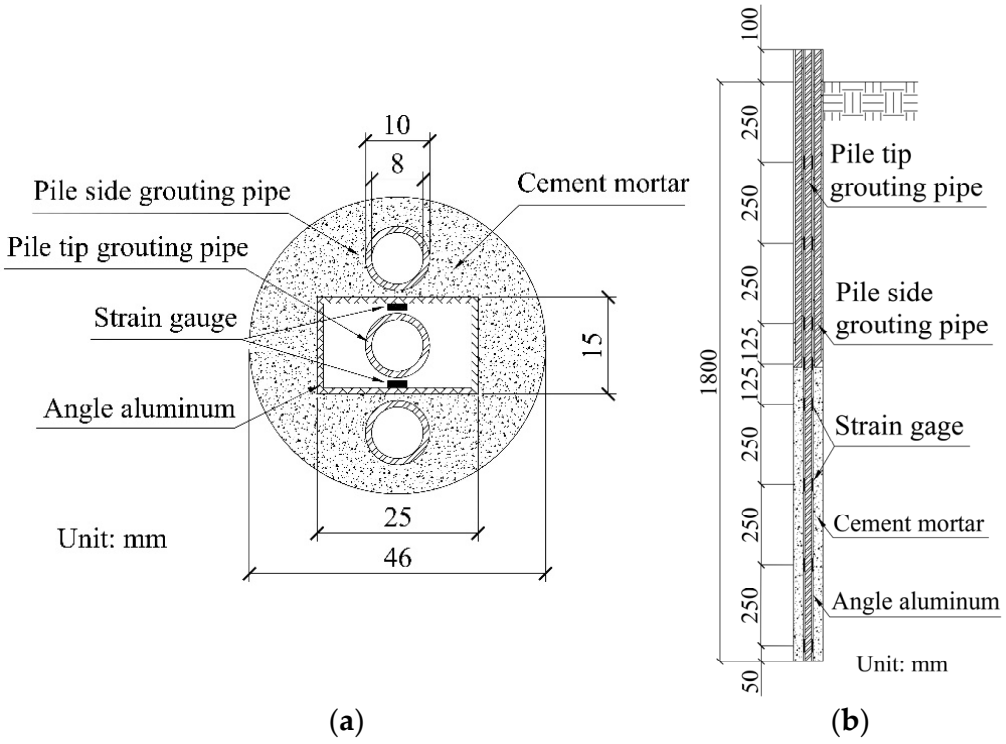


Figure 2. Schematic diagram of model pile design. (**a**) Pile section; (**b**) pile profile diagram.

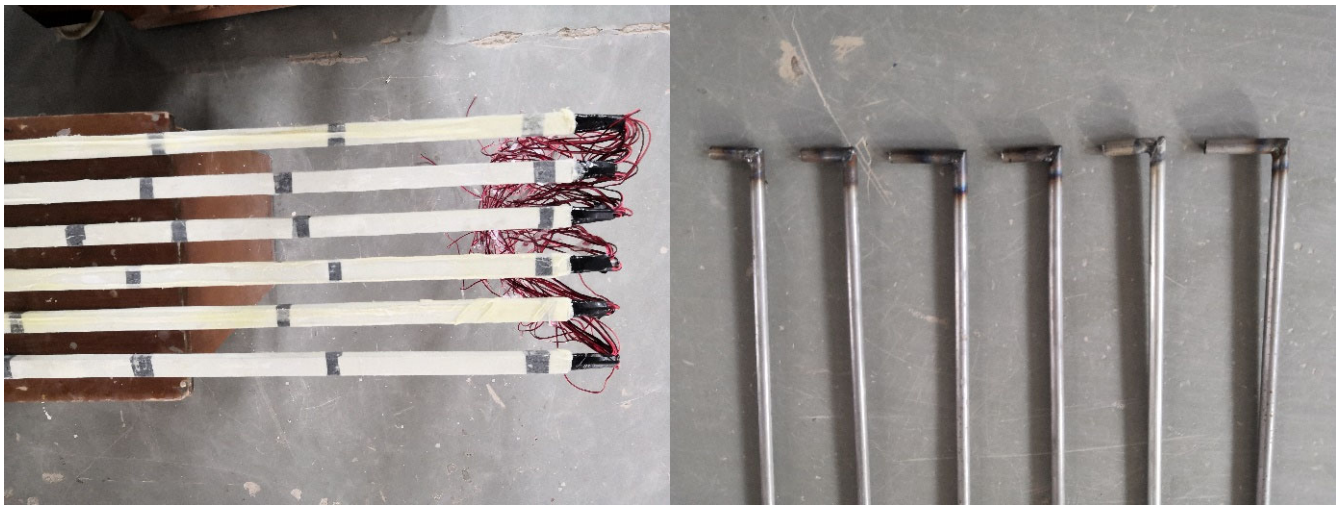


Figure 3. Pile core making and side grouting pipe-end treatment. (**a**) Pile cores; (**b**) side grouting pipes.

The model pile was equipped with three grouting pipes, including one tip grouting pipe and two side grouting pipes, made of seamless steel tubes (the model pile used for pile-tip grouting is equipped with only one tip grouting pipe). The grouting pipe has an

outer diameter and thickness of 10 mm and 1 mm, respectively. The tip grouting pipe runs through the entirety of the pile core, while the two side grouting pipes are symmetrically attached to the long edge of the pile core. In particular, each pile side grouting pipe was meticulously welded to establish a connection between the pipe section and the outlet section, ensuring that the outlet direction remains perpendicular to the axis of the pile body, as shown in Figure 3b. The distance between the pile side grouting outlet and the soil surface measures 0.875 m. Additionally, a pair of strain gauges have been affixed at the horizontal position of the pile side grouting outlet to facilitate the monitoring of internal forces.

The casting template for the model pile was made from a PVC pipe with a 50 mm outer diameter and 2 mm thickness. The cement mortar mixture used for pile casting consisted of water, cement, and fine sand in the ratio of 0.6:1.0:2.5. After the completion of casting a model pile, it was maintained in the PVC mold for 28 days. Subsequently, the mold was removed, the excess grouting pipes were cut off, and the uneven parts of the pile body were ground flat. Figure 4 presents the curing and post-treatment of model piles.



(**a**) (**b**)

Figure 4. Curing and post-treatment of model piles. (**a**) Curing of model piles; (**b**) excision of the excess steel pipe.

2.3. Elastic Modulus of Model Piles

Elastic modulus is an important parameter for calculating the compression of the pile body during experimental analysis. As individual differences can arise during the casting process of the model pile, the elastic modulus of each pile was individually determined in this study. The basic method for elastic modulus determination is based on the fundamental assumptions of material mechanics: assuming that the model pile conforms to the cross-section assumption in compression and bending. The method is as follows: (1) setting two side supports with equal height and a certain distance apart, supporting the two ends of a certain model pile, and setting the two side supports 50 mm away from the pile end on each side, as shown in Figure 5; (2) setting a dial gauge at the center of the pile to record the central deflection of the pile; (3) gradually loading the pile by hanging weights at the center of the pile, with load values of 5 N, 10 N, 15 N, 20 N, and 25 N; (4) substituting the measured load values and deflection values into the equation to calculate the elastic modulus:

$$E_{\mathrm{p}} = \frac{\Delta P L^3}{48 \Delta f I_{\mathrm{p}}} \tag{1}$$

where E_{p} is elastic modulus, ΔP is the load value of each level, L is the effective length of the pile, L is 1.8 m in this study, Δf is pile center deflection corresponding to each level of load, and I_{p} is the inertia moment of pile section.



Figure 5. Measurement of elastic modulus of the model pile.

2.4. Filling, Unloading, and Arrangement of Model Piles

During the filling process, uniform filling of the soil was carried out in layers of 20 cm, starting from the bottom of the model chamber. Each layer of soil was filled at intervals of 0.5 h to allow for sufficient compaction under self-weight consolidation. This process continued until the soil reached the desired elevation at the top of the model chamber.

Previous research has demonstrated that the drilling and unloading of cast in situ piles can lead to a decrease in the lateral friction resistance of piles and ultimately reduce the ultimate bearing capacity [2,34,35]. Therefore, to account for the impact of unloading on experimental outcomes, this study conducted simulations of soil unloading during testing. Specifically, PVC pipes were initially embedded in the soil and subsequently replaced with model piles. Over time, the surrounding soil pressure partially recovered, resulting in a certain degree of unloading around the model piles.

In a pile model test, a certain distance condition of pile spacing needs to be satisfied to avoid mutual influence and interference with the test results. Previous studies have shown that the interactions between the pile and the test chamber wall and among the piles cannot be ignored until the distance exceeds 6 D and 3 D, respectively, where D represents the pile diameter [33,36]. In this study, a total of 14 model piles were designed for testing. Figure 6 shows the specific arrangement scheme of model piles, where the minimum distance between the chamber wall and piles was 0.310 m (6.74 D), while the minimum pile spacing was 0.370 m (8.04 D). Therefore, each model pile can be considered an independent entity (single pile) for analysis purposes.

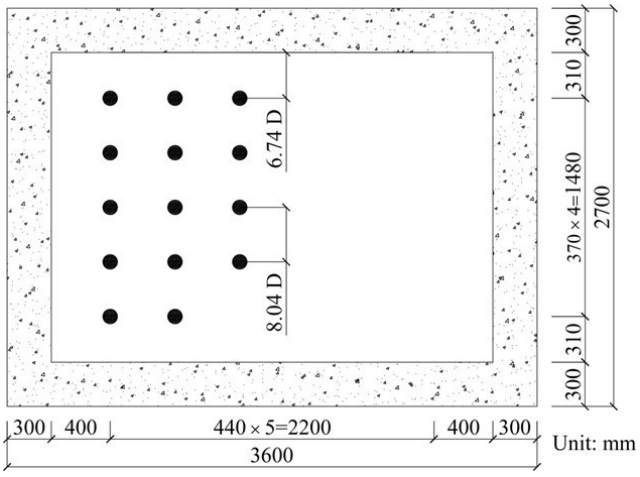


Figure 6. Arrangement of model piles.

2.5. Post-Grouting and Loading

The study employs a grouting device consisting of various components, such as an air compressor, pressure-regulating valves, a grout storage tank, a grout inlet pipe, and a pressure gauge, as depicted in Figure 7. The pressure-regulating valve is used to maintain a stable pressure to facilitate the injection of a defined volume of cement grout from the grout storage tank into the pile tip or side grouting pipe. Considering the strength of the cement-stabilized soil surrounding the piles and the consistency of cement grout, ordinary Portland cement (P.O.) 42.5 with a water–cement ratio of 0.6 was selected as the grouting material for the study.

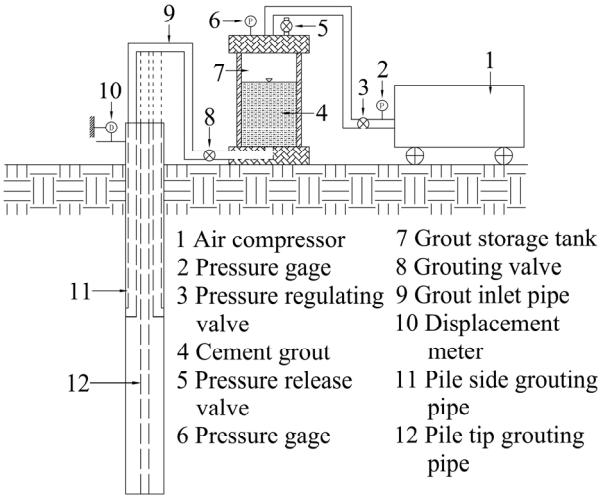


Figure 7. Grouting device.

The experimental loading method involves converting the gravitational force of certain weights into a vertical load applied to the pile top by utilizing steel tracks and pulley blocks. The loading device diagram is shown in Figure 8. Dial gauges and strain gauges were used to record the settlement of the pile top and deformation data of the pile body, respectively. The loading process utilized the rapid maintenance load method, which follows the "Technical code for testing of building foundation piles" of China (2014). Pile top displacement data were recorded at 0, 5, 10, 15, and 30 min after each level of the load was applied (and every 15 min thereafter). When the difference between the two displacements is less than 0.01 mm, the pile is considered to be stable, and the next level of load continues to be applied. The criterion for stopping loading is that the pile top displacement under one level of load is more than 5 times that of the previous level. The ultimate bearing capacity of the model pile is the load value of the previous stage.

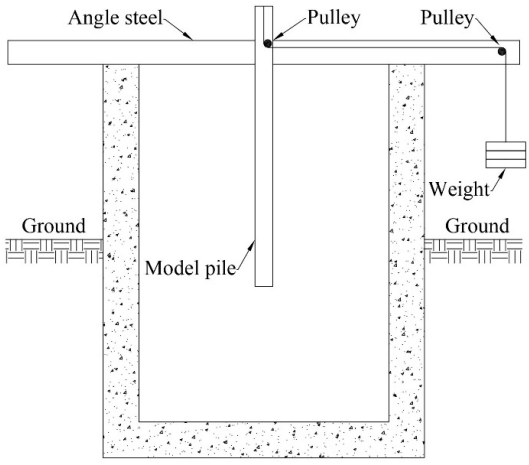


Figure 8. Loading device.

2.6. Test Groups

This study mainly considers the grouting form, grouting volume, and grouting pressure as the studied variables, based on which each pile is numbered. Table 2 presents the group design of 14 model piles. The model piles are divided into four groups based on the grouting form: non-grouting, tip grouting, side grouting, and combined grouting. For the grouting volume, except for the non-grouting group, the total grouting volume of each group of piles is set to three levels: 1, 2, and 3 L. For pile-side grouting, the volumes of cement grout injected into the two side grouting pipes are identical. For instance, in S36, the volume in each side grouting pipe is 1.5 L. In combined grouting, the volumes of pile tip and side grouting are equivalent. For example, in TS36, the volume of each side grouting pipe is 0.75 L and that of the tip grouting pipe is 1.5 L. According to the results of the preliminary experiment and the injectability of the grout, the grouting pressure of the basic control group is set to 0.6 MPa. In addition, a comparative design with grouting pressures of 0.5 MPa and 0.7 MPa is added to the tip grouting group and the side grouting group, respectively.

Table 2. Test groups.

Group Number	Grouting Form	Pile Number	Grouting Volume/L	Grouting Pressure/MPa
1	Non-grouting	N00	0	0
2	Pile tip grouting	T16	1	0.6
		T26	2	0.6
		T36	3	0.6
		T25	2	0.5
		T27	2	0.7
3	Pile side grouting	S16	1	0.6
		S26	2	0.6
		S36	3	0.6
		S25	2	0.5
		S27	2	0.7
4	Combined grouting	TS16	1	0.6
		TS26	2	0.6
		TS36	3	0.6

3. Test Results and Analysis

3.1. Pile Top Load–Settlement Relationship

The ultimate bearing capacity of each pile and the corresponding pile top settlement are listed in Tables 3–5. Figure 9 presents the pile top load–settlement relationship of model piles with different grouting volumes. In terms of the trend of curves, the load–settlement relationship of each pile is approximately linear at low loads, while the curve gradually becomes nonlinear until it reaches the ultimate bearing capacity. In each grouting group, the length of the linear segment is significantly longer than that of the non-grouted pile (N00), indicating the enhancement of bearing stiffness with grouting. The final settlement of almost all piles was found to be considerable due to the limited support provided by cohesive soils compared to sandy soil formations. The test results revealed that several piles experienced sudden collapse upon surpassing their ultimate bearing capacity, emphasizing the need to consider potential failure modes in the design and construction of pile foundations in cohesive soils.

The ultimate bearing capacity of N00 is 0.8 kN, while post-grouting significantly increases the ultimate bearing capacity. Furthermore, from Tables 3–5, it can be observed that, as the grouting volume increases, the improvement in the ultimate bearing capacity of the pile becomes more pronounced. As the grouting volume increased from 1 L to 3 L, the bearing capacity of the pile tip, pile side, and combined grouting group increased from 1.6 kN, 4.4 kN, and 4.4 kN to 5.7 kN, 7.3 kN, and 7.9 kN, respectively. In terms of pile top settlement, the ultimate settlement of N00 is 3.86 mm. Except for pile T16, all

grouting piles have borne more than 3 kN load when reaching this settlement. Therefore, post-grouting can reduce the pile-top settlement remarkably. As shown in Figure 9, when the grouting volume is 1 L, the ultimate bearing curve decreases from N00 for all grouting forms. This indicates that the reinforcement effect of grouting on the soil–pile system is not strong enough when the grouting volume is relatively small, resulting in significant pile displacement under large ultimate loads. The ultimate bearing capacity curve shows a significant upward trend after the grouting volume reaches 2 L, indicating that an adequate grouting volume is more favorable for controlling the pile settlement.

Table 3. Ultimate bearing capacity and pile top settlement for the tip grouting group.

Pile Number	T16	T26	T36	T25	T27
Ultimate bearing capacity/kN	1.6	3.4	5.7	4.8	6.0
Pile top settlement/mm	11.38	3.97	8.90	2.93	9.65

Table 4. Ultimate bearing capacity and pile top settlement for the side grouting group.

Pile Number	S16	S26	S36	S25	S27
Ultimate bearing capacity/kN	4.4	5.2	7.3	6.4	6.7
Pile top settlement/mm	5.17	2.24	1.86	3.47	2.50

Table 5. Ultimate bearing capacity and pile top settlement for the non-grouting and combined grouting group.

Pile Number	N00	TS16	TS26	TS36
Ultimate bearing capacity/kN	0.8	4.4	6.4	7.9
Pile top settlement/mm	3.86	14.62	5.75	6.94

Figures 10 and 11 present the variation curves of ultimate bearing capacity and settlement concerning the grouting form and grouting pressure. As shown in Figure 10, under the condition of the same volume of grout, the ultimate bearing capacity curve of the grouting pile shows an upward trend from pile tip grouting to pile side grouting and then to combined grouting. The reason for this can be attributed to the relatively small lateral friction and tip-bearing resistance of the pile in cohesive soils with shallow depths. Therefore, single grouting at either the pile tip or pile side is unable to effectively reinforce the contact surface between the pile and soil on both sides. In contrast, combined grouting, although with a reduced grout volume from individual grout ports, has a wider reinforcement coverage around the pile. Moreover, the reinforcing effect on the soil around the pile is more pronounced on the pile side than on the pile base. The ultimate pile-top settlement of the pile-side grouting group is much smaller than the other two grouting groups, indicating that pile-side grouting greatly improves the shear performance of the soil around the pile and reduces the pile–soil relative displacement.

In the pile tip and pile side grouting groups, the ultimate bearing capacity exhibits a decreasing then increasing trend as the grouting pressure increases from 0.5 MPa to 0.6 MPa and 0.7 MPa. Regarding the ultimate settlement, the pile tip grouting group shows a positive correlation with grouting pressure, while the pile side grouting group has a negative correlation. Therefore, the influence of grouting pressure does not exhibit a particularly clear pattern in terms of the load–settlement relationship.

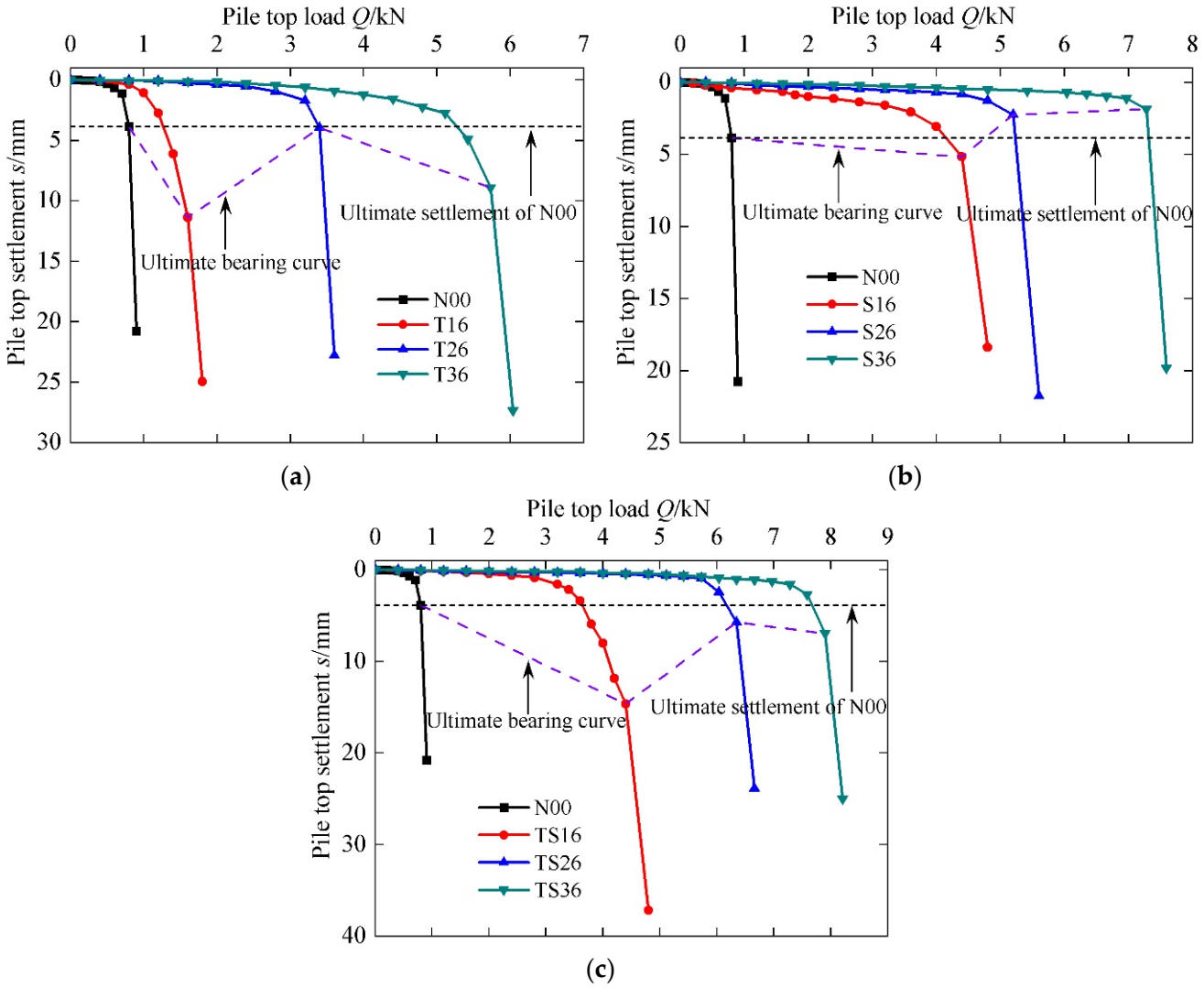


Figure 9. Pile top load–settlement relationship with different grouting volumes. (**a**) Pile tip grouting group; (**b**) pile side grouting group; (**c**) combined grouting group.

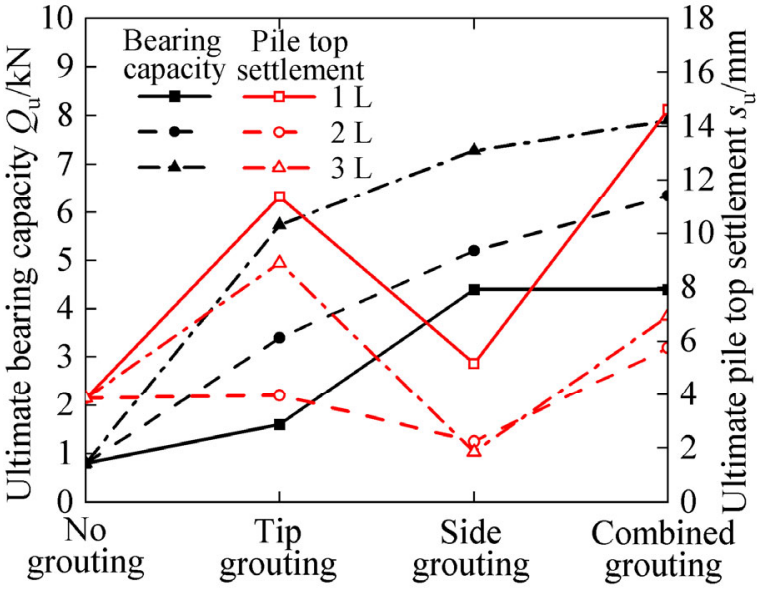


Figure 10. Ultimate bearing capacity and pile top settlement under different grouting forms.

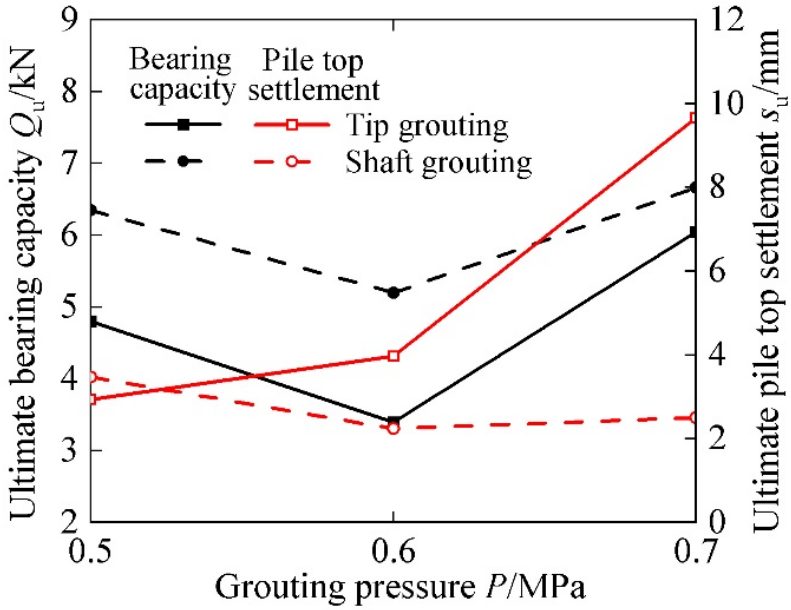


Figure 11. Ultimate bearing capacity and pile top settlement with different grouting pressures.

3.2. Pile Top Load–Settlement Relationship

A model pile can be divided into several sections according to the position of strain gauges. Pile axial force N_i at section i is:

$$N_i = E_p \varepsilon_i A_p \tag{2}$$

where E_p is elastic modulus of each pile, which was measured separately, ε_i is section strain, and A_p is section area.

The average lateral friction resistance of a certain section τ_{si} can be expressed as:

$$\tau_{si} = \frac{N_{i-1} - N_i}{A_i} \tag{3}$$

where A_i is the lateral area of the pile section.

Figures 12 and 13 illustrate the distributions of ultimate pile lateral friction resistance for different grouting groups. The pile lateral friction resistance at each depth of N00 is below 3.0 kPa, while the lateral friction resistances of some sections near grouting outlets of grouted piles are significantly enhanced. The grout will spread along the pile–soil surface, resulting in the soil near a grouting outlet being strengthened first. The enhancement of a section of the same grouting group is proportional to the grouting volume. A sufficient volume of grout can fully fill the weakening pile–soil surface, resulting in denser soil cement within the range of grout reinforcement, which can improve shear performance. Except for some pile sections out of reinforcement areas, an increase in grouting volume will lead to an increase in pile lateral friction.

As shown in Figure 12a, in the context of pile tip grouting, the value of pile lateral friction resistance increases as the distance to the pile tip decreases, reaching a range of 13.5 kPa to 42.8 kPa within a depth of 1.50 m to 1.75 m. According to the reinforcement effect of cement grout on pile skin friction, the diffusion range of cement grout is independent of grouting volume and ranges from a depth of 1.25 m to 1.75 m. However, the lateral friction resistance of the upper part of each pile with tip grouting is similar to that of N00 and has little effect on the bearing capacity. As shown in Figure 12b, the grout diffusion range of the pile side grouting group ranges from 0.50 m to 1.75 m in depth, which is more comprehensive than the coverage of pile tip grouting. The reinforcement range of grout on the pile side below the outlet is obviously larger than that above the outlet (the location of the pile side outlet is 0.875 m deep), which indicates that the downward

diffusion range of grout is greater than that of the upward diffusion. The reason for this phenomenon is that the setting of pile–soil unloading makes the grout preferentially split downward under the action of gravity. With the increase in grouting volume from 1 L to 3 L, the maximum value of pile shaft resistance reaches 32.6~54.2 kPa, all of which are located at the pile side grouting outlet. The pile lateral friction resistance decreases with the increase in the distance from the outlet. As depicted in Figure 12c, the pile lateral friction resistance distribution of the combined grouting group exhibits both of the aforementioned characteristics, with the larger value of pile lateral friction resistance located near the pile side grouting outlet and pile tip.

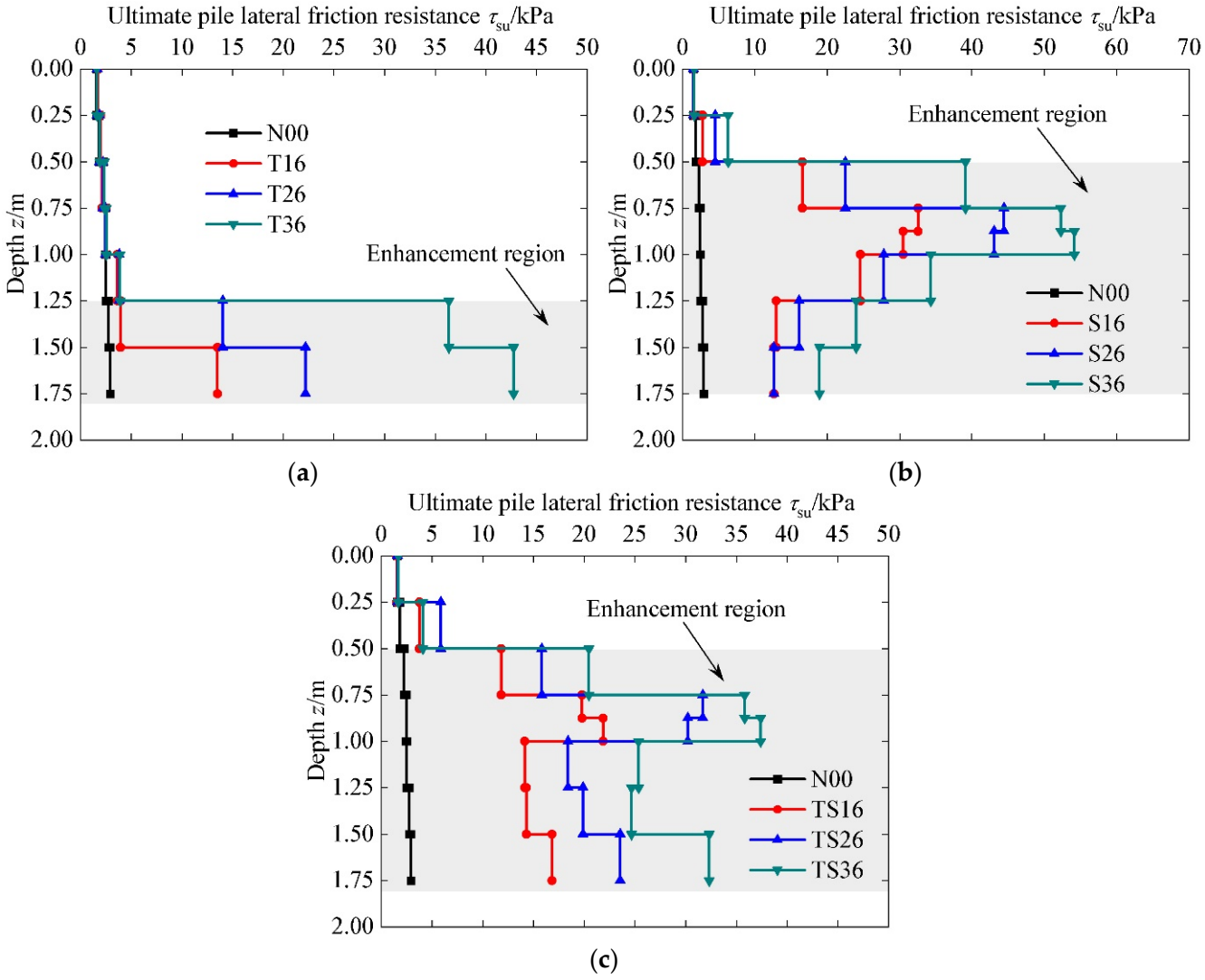


Figure 12. Distribution of ultimate pile lateral friction resistance with different grouting volumes. (**a**) Pile tip grouting group; (**b**) pile side grouting group; (**c**) combined grouting group.

Figure 13 shows the ultimate pile lateral friction distribution of the tip grouting pile and side grouting pile with different grouting pressures. There is no great change in the pile side lateral reinforcement enhancement region when the pressure changes from 0.5 MPa to 0.7 MPa. The influence of different grouting pressures on the lateral resistance is not obvious.

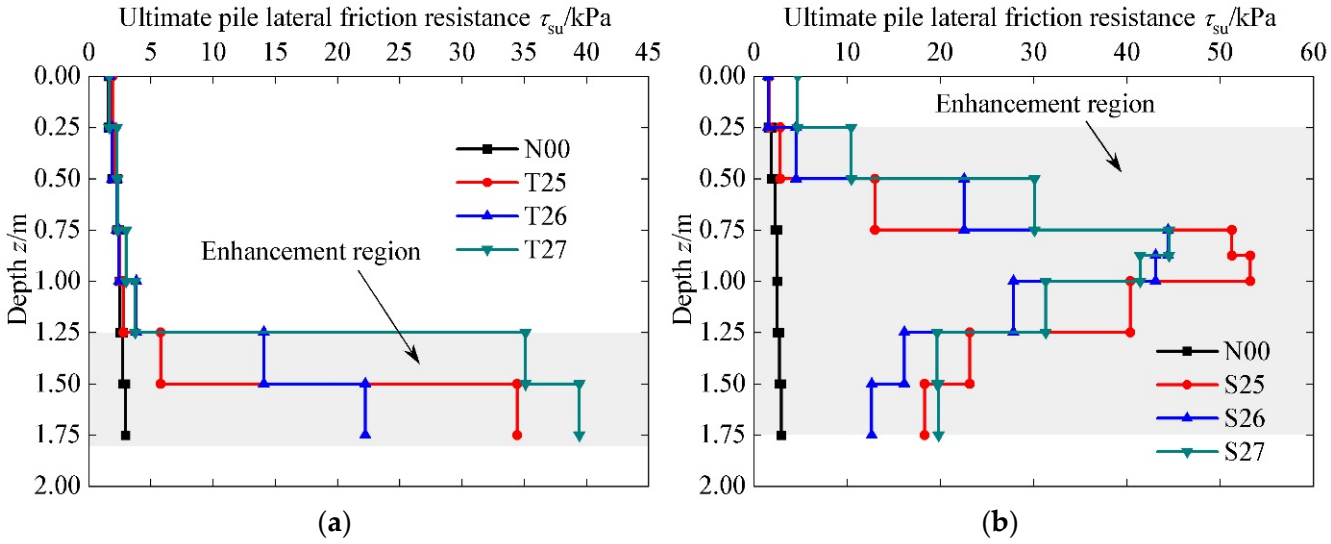


Figure 13. Distribution of ultimate pile lateral friction resistance with different grouting pressures. (**a**) Pile tip grouting group; (**b**) pile side grouting group.

3.3. Ultimate Pile Tip Resistance

The tip resistance value of each pile can be estimated through the axial force value measured by the strain gauge at the bottom to investigate how various grouting conditions affect the ultimate pile tip resistance. The findings are presented in Figure 14, which shows that pile N00's ultimate tip resistance is 0.21 kN, accounting for 25.9% of the pile top load. The authors also found that the tip resistance of the pile side grouting group ranged from 0.54 kN to 0.87 kN, which indicates that grout diffuse to the pile bottom from the pile side outlet, but the effect on the pile tip resistance is limited. In contrast, the tip resistance of pile tip grouting and combined grouting group had a positive correlation with grouting volume, which increased from 0.53 kN and 1.39 kN to 2.43 kN and 2.65 kN, respectively, as grouting volume increased from 1 L to 3 L. The actual grouting efficiency was found to be better in the combined grouting group, where the grouting volume at the pile tip only accounted for half of the total grouting volume.

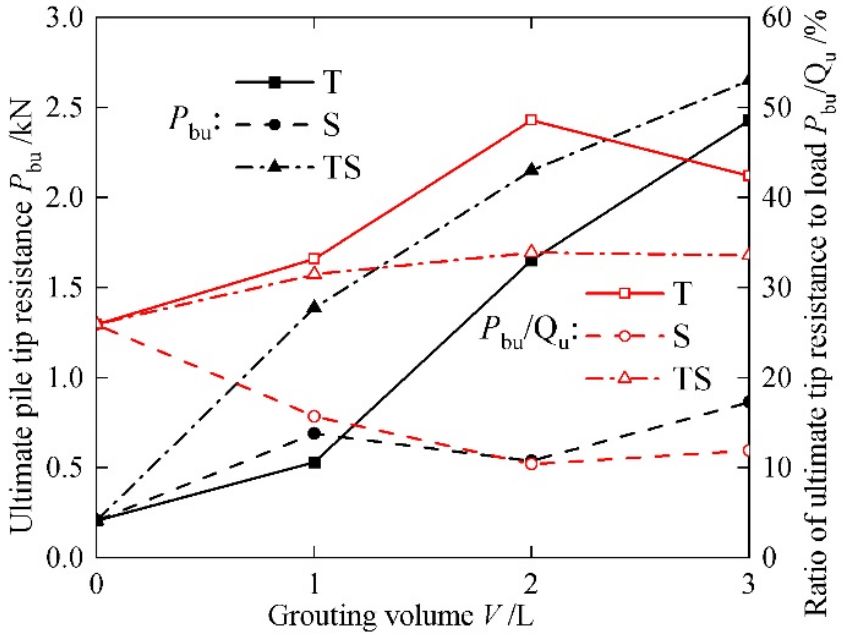


Figure 14. Ultimate pile tip resistance and the ratio of ultimate pile tip resistance to load.

The transfer efficiency of a load can be represented by the ratio of pile tip resistance to the ultimate load. The bearing ratio of the pile side grouting group was kept at a low level (10.4~15.7%) due to the large lateral friction resistance, while the bearing ratio of the combined grouting group was stable between 31.5% and 33.9%. The authors also found that pile lateral friction resistance and tip resistance increased synchronously with the increase in grouting volume. Regarding pile tip grouting, the bearing ratio initially increased to 48.6% and then decreased to 42.4% with the change in grouting volume, indicating that the return of grout had a greater effect on lateral friction resistance when the grouting volume was large. The insufficient tip resistance of T16 was attributed to factors such as soil compactness at the pile bottom, grouting details, and grout diffusion.

4. Discussion of Grout Diffusion and Reinforcement

Following the experiment, model piles were excavated from the test chamber. The appearance of a portion of model piles after excavation is depicted in Figures 15–18. Some parts of the grouted piles exhibited a significant amount of grout–soil mixture or grouting marks. By conducting measurements and analyses, the diffusion and reinforcement characteristics of grouting under different forms can be examined in terms of grouting diffusion range and pile–soil failure mechanism. It is crucial to acknowledge that the thickness of the soil in the scaled model tests and, correspondingly, the stress field within the soil are considerably smaller than those observed in real-world engineering scenarios. Consequently, the impact of soil stress on grout confinement during the grouting process is diminished, leading to a wider dispersion range of the grout. Thus, the conclusions drawn regarding grout diffusion in this study should be regarded solely as qualitative observations and analyses [37]. Furthermore, the experiment did not include instruments to monitor the stress state of the soil [38], making it challenging to quantify the compaction effects of grouting on the soil. The enhancement of pile side resistance due to grouting can only be analyzed from the perspective of improved shear performance of the grouted region.

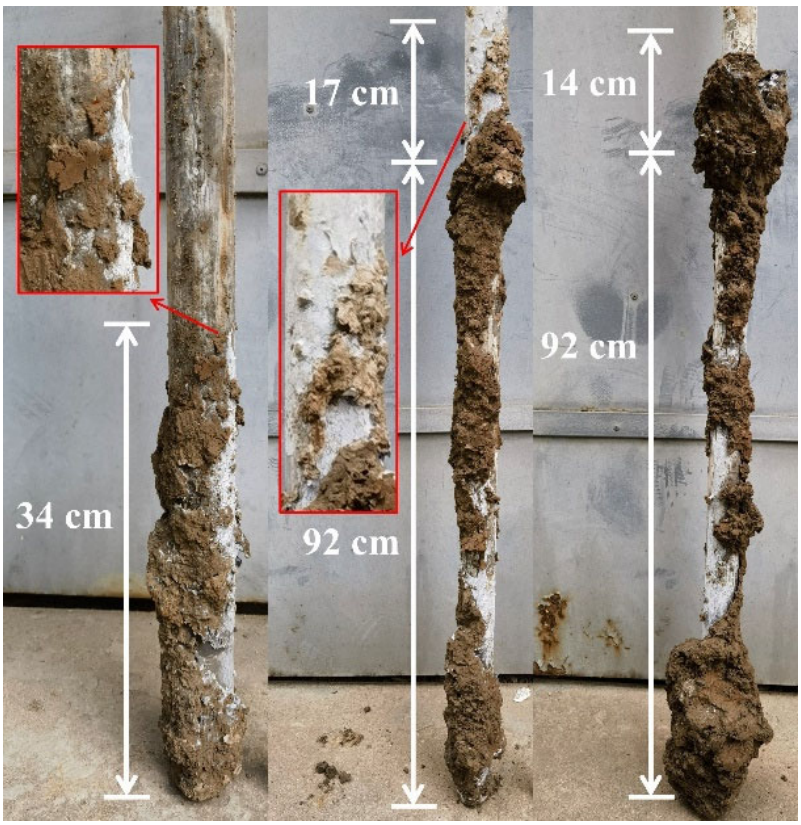


Figure 15. Grout vertical diffusion range of piles T26, S26, and TS26.

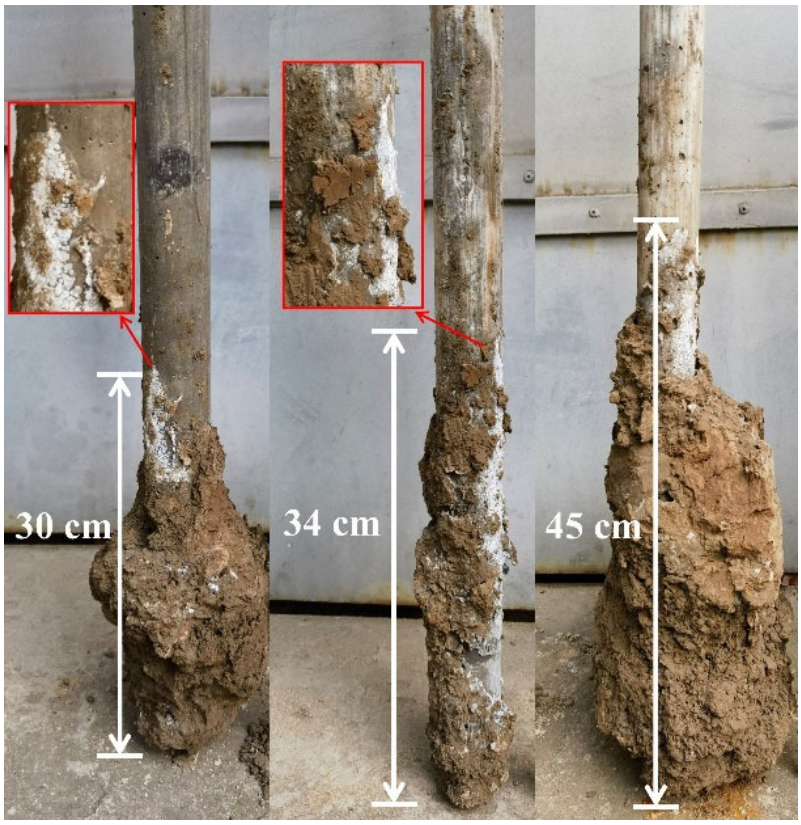


Figure 16. Grout vertical diffusion range of piles T25, T26, and T27.

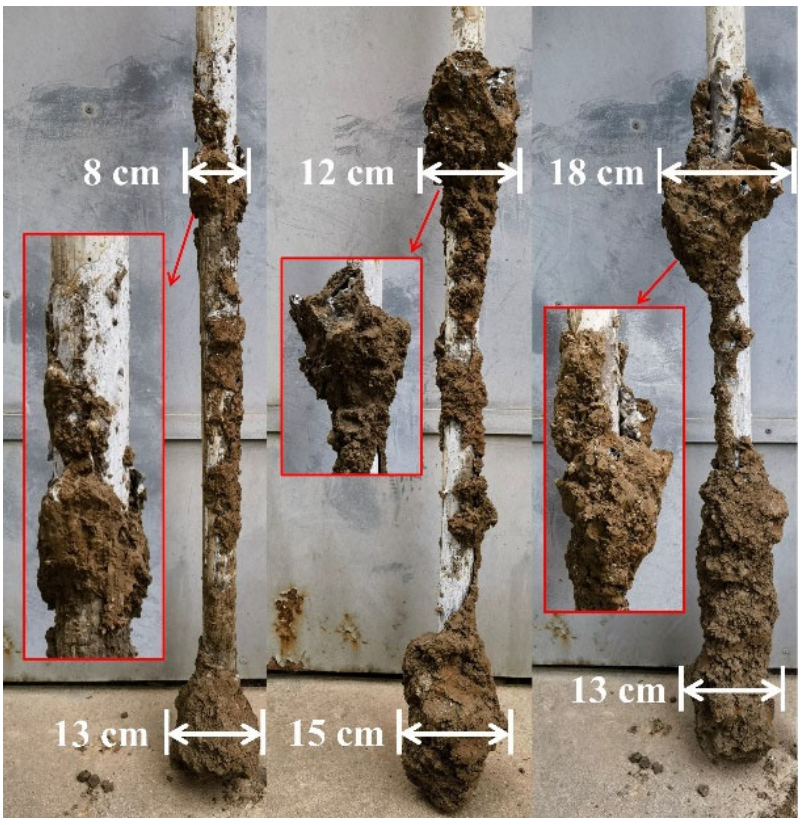


Figure 17. Grout horizontal diffusion height of piles TS16, TS26, and TS36.



Figure 18. Pile side grout body of pile TS26.

4.1. Grout Vertical Diffusion Range

The area surrounding a grouted pile, which is formed by the interaction of grout and soil, comprises two distinct regions: grout accumulation at the grouting outlet and grout splitting diffusion along the pile body. For vertical grout diffusion, Figure 15 displays the results of grout diffusion measurements along vertical lines for different grouting forms. In pile T26, the grout diffusion height is 34 cm (7.4 D) above the pile tip, while, in S26, the diffusion range extends almost from the side outlet to the pile end and reaches 17 cm above the side outlet. The height of grout diffusion downward is significantly greater than that of upward diffusion, whereas the diffusion height upward is lower than that of the tip-grouted pile. This is because a weak stress zone is formed at the pile–soil interface under the influence of soil unloading, causing the grout to preferentially split and spread downward under gravity. The results of side-grouted pile TS26 are similar, with a notably smaller height of upward diffusion. And the grouting fluid used for tip and side grouting is connected. The results of each pile subjected to tip grouting under different pressures are shown in Figure 16. Notably, the return height of grout in tip-grouted piles varies significantly with grouting pressure. Concretely, when the grouting pressure is 0.5, 0.6, and 0.7 MPa, the grout return height is 30, 34, and 45 cm (6.5 D, 7.4 D, and 9.8 D), respectively. In contrast, the diffusion range of S25 and S27 is similar to that of S26. Although it is generally believed that factors such as pile diameter, depth, grouting pressure, and grout type affect the diffusion height of grout, the test results indicate that soil unloading also has a substantial impact on grout diffusion range, particularly in the context of side-grouted piles. It is worth noting that there is a strong correlation between the grout diffusion height and the range of lateral friction enhancement. Taking pile TS26 as an example, the measured coverage of grout extends from 14 cm above the side grout outlet to the bottom of the pile. Meanwhile, the lateral friction enhancement segment of the pile is from approximately 30 cm above the side grout outlet to the bottom of the pile. Considering the precision of 25 cm for the height interval of the side friction regions, the range of grout diffusion and the range of side friction enhancement overlap significantly.

4.2. Grout Horizontal Diffusion Range

As an illustration of combined grouting at the pile tip and pile side, Figure 17 presents the measurement results of the horizontal diffusion range of grout for three combined grouting piles subjected to different grouting volumes. Large spherical or ellipsoidal cement grout bodies were formed at the pile tip and pile side outlets. The width of the grout body at the pile tip ranges from 13 cm (2.8 D) to 15 cm (3.3 D), whereas that at the pile side outlet ranges from 8 cm (1.7 D) to 18 cm (3.9 D). Specifically, the pile side grout body of TS16 sustained partial damage. Notably, as the grouting volume increases, both the horizontal and vertical dimensions of the grouting body at the pile tip and pile side increase, thereby explaining the reason for the ultimate pile lateral friction resistance at the same position increase from TS16 to TS26 and TS36 in Figure 12. In the area between the pile tip and the pile side outlet, the thickness of the grout residue was significantly smaller than that at the outlet, measuring less than 2 cm. In the distribution curve of lateral friction resistance shown in Figure 12, a significant increase in lateral friction is observed at grouting outlets. This indicates that the formation of grout body greatly enhances the lateral friction resistance of a pile.

4.3. Grout Diffusion and Pile–Soil Failure Mechanism

Figure 18 displays the top and front views of the pile side grout body of pile TS26. The grout body is composed of solidified cement grout and soil mass. The cement grout appears as a dense block near the pile, while, on the outside of the grout body, several traces of broken grout veins are embedded in the soil. This indicates that, during the grouting process, a grout bubble is formed near the outlet, and splitting occurs on the outer side of the bubble due to higher grout pressure than the splitting pressure of soil. With the continuous injection of grout, a certain size compaction zone is formed inside the bubble. The final size of the grout body is related to the grouting volume. Furthermore, the cement grout spreads along the axial splitting of the pile body to form a particular reinforcement area. The grout diffusion diagram for pile tip, pile side, and combined grouting is presented in Figure 19.

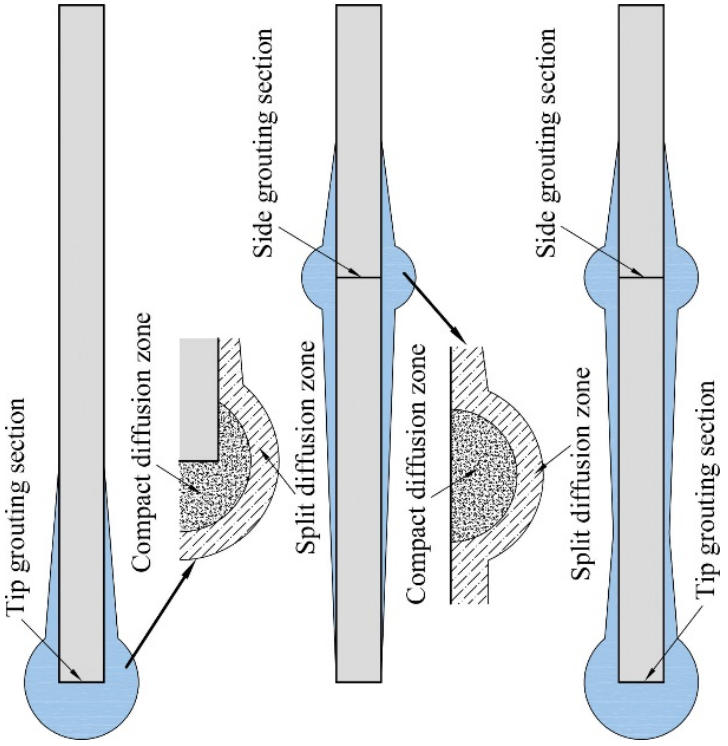


Figure 19. Grout diffusion diagram of pile tip, pile side, and combined grouting.

There are two primary modes of pile–soil failure. The first occurs either in or outside the splitting diffusion zone of the grout body (as exemplified by the side grout body of pile TS26), while the second occurs between the pile and the grout (as exemplified by the side grout body of pile TS16). The ultimate lateral friction resistance of piles TS26 and TS16 is 30.2~31.7 kPa and 19.8~21.9 kPa, respectively, at a depth of 0.75 m to 1.00 m. This indicates that the ultimate friction resistance of the pile lateral under the first failure mode is significantly higher than that under the second failure mode. For instance, the grout body of pile T27 is relatively intact, while that of pile T26 is partially destroyed, explaining why the ultimate pile lateral friction resistance of T27 at a depth of 1.50 m to 1.75 m is 39.5 kPa, which is higher than that of T26 at 22.2 kPa. The second failure mode typically occurs in areas away from the grouting outlet, and the primary reason for this is that the combination of grout and pile is less dense than that at the outlet.

5. Conclusions

This paper presents the conclusions drawn from model tests conducted on grouting and static load to study the single pile-bearing capacity under conditions of unloading and different grouting parameters. The main findings are summarized as follows:

(1) Increasing the grouting volume has a favorable impact on the ultimate bearing capacity for both pile tip, pile side, and combined grouting piles. Pile side grouting is more beneficial to control pile settlement. From a grouting efficiency perspective, combined grouting demonstrates superior reinforcement effects compared to the other two grouting methods. The influence of different grouting pressures on bearing characteristics is not significantly apparent.

(2) Following grouting, a lateral friction resistance enhancement region is formed near the grouting outlet, extending to a certain height. Within this region, the pile's lateral friction resistance shows a negative correlation with the distance from the grouting outlet. Both pile lateral and tip resistance exhibit a positive correlation with the grouting volume.

(3) Post-grouting results in the formation of a grout bubble at the outlet, with a compact diffusion zone on the inside and a split diffusion zone on the outside. The size of the grout bubble demonstrates a positive correlation with the grouting volume. Another portion of the grout diffuses vertically along the pile–soil interface from the grouting outlet, creating a reinforcement zone. Combined grouting piles exhibit the widest range of grouting fluid diffusion, enabling the connection of reinforcement areas at the pile tip and pile side. As grouting pressure increases from 0.5 MPa to 0.6 MPa and 0.7 MPa, the grout return height rises from 6.5 D to 7.4 D and 9.8 D. However, the relationship between pile side grouting height and pressure is less pronounced due to considerations of the unloading effect.

(4) Two primary modes of pile–soil failure are observed. The first mode involves failure either within or outside the split diffusion zone of the grout body, typically occurring near the outlet. The second mode of failure occurs between the pile and the grout, generally at a location away from the grouting outlet. The ultimate pile lateral friction resistance under the first failure mode is significantly higher than that under the second failure mode.

Author Contributions: Conceptualization, J.Z. and C.Z.; methodology, J.Z. and Y.W.; software, J.Z.; validation, J.Z., C.Z., and Y.W.; formal analysis, J.Z.; investigation, J.Z.; resources, C.Z.; data curation, J.Z.; writing—original draft preparation, J.Z.; writing—review and editing, J.Z., C.Z., and Y.W.; visualization, J.Z.; supervision, J.Z. and C.Z.; project administration, J.Z.; funding acquisition, C.Z. and Y.W. All authors have read and agreed to the published version of the manuscript.

Funding: This research was funded by the National Natural Science Foundation of China (Grant Nos. 42377151), the Natural Science Foundation of Chongqing (CSTB2023NSCQ-BHX0149), and the China Postdoctoral Science Foundation (2023MD734112).

Institutional Review Board Statement: Not applicable.

Informed Consent Statement: Not applicable.

Data Availability Statement: The data of this study are available from the corresponding author upon reasonable request.

Conflicts of Interest: The authors declare no conflict of interest.

References

1. Hu, H.; Jin, Q.; Yang, F.; Zhou, J.; Ma, J.; Gong, X.; Guo, J. A Novel Method for Testing the Effect of Base Post-Grouting of Super-Long Piles. *Appl. Sci.* **2022**, *12*, 10996. [CrossRef]
2. Wu, Y.; Zhang, X.F.; Zhao, C.; Zhao, C.F. Effects of soil unloading and grouting on the vertical bearing mechanism for compressive piles. *Ocean Eng.* **2023**, *271*, 13. [CrossRef]
3. Zheng, X.; Shi, B.; Sun, M.; Wang, X.; Wang, K.; Ni, W. Evaluating the effect of post-grouting on long bored pile based on ultra-weak fiber Bragg grating array. *Measurement* **2023**, *214*, 99. [CrossRef]
4. Zhao, C.; Zhang, J.; Zhao, C.; Wu, Y.; Wang, Y. Cavity reverse expansion considering elastoplastic unloading and application in cast-in-situ bored piles. *Soils Found.* **2023**, *63*, 101339. [CrossRef]
5. Hu, T.; Dai, G.; Wan, Z.; Gong, W.; Fang, B. Field study of the effects of composite excavation and combined grouting on the response of large-diameter and superlong rock-socketed bored piles. *Acta Geotech.* **2023**, *116*, 1–19. [CrossRef]
6. Thiyyakkandi, S.; McVay, M.; Bloomquist, D.; Lai, P. Experimental study, numerical modeling of and axial prediction approach to base grouted drilled shafts in cohesionless soils. *Acta Geotech.* **2014**, *9*, 439–454. [CrossRef]
7. Xue, Z.; Feng, H.; Ren, C.; Zhou, Z. Model test of lateral and end combined grouting of bridge cast-in-place pile foundation in Loess Area. *J. Chang. University. Nat. Sci. Ed.* **2021**, *41*, 19–28.
8. Fleming, W.G.K. The improvement of pile performance by base grouting. *Proc. Inst. Civ. Eng. Civ. Eng.* **1993**, *97*, 88–93. [CrossRef]
9. Joer, H.A.; Randolph, M.F.; Gunasena, U. Experimental modeling of the shaft capacity of grouted driven piles. *Geotech. Test. J.* **1998**, *21*, 159–168.
10. Mullins, G.; Winters, D.; Dapp, S. Predicting end bearing capacity of post-grouted drilled shaft in cohesionless soils. *J. Geotech. Geoenviron. Eng.* **2006**, *132*, 478–487. [CrossRef]
11. Wan, Z.; Dai, G.; Gong, W. Field study on post-grouting effects of cast-in-place bored piles in extra-thick fine sand layers. *Acta Geotech.* **2019**, *14*, 1357–1377. [CrossRef]
12. Zou, J.; Yang, T.; Deng, D. Field test of the long-term settlement for the post-grouted pile in the deep-thick soft soil. *Geomech. Eng.* **2019**, *19*, 115–126.
13. Bolognesi, A.J.L.; Moretto, O. Stage grouting preloading of large piles on sand. In Proceedings of the 8th International Conference on Soil Mechanics and Foundation Engineering, Moscow, Russia, 6–11 August 1973; pp. 19–25.
14. Bustamante, M.; Gouvenot, D. Grouting: A method improving the bearing capacity of deep foundation. In Proceedings of the 8th European Conference Soil Mechanics and Foundation Engineering, Helsinki, Finland, 23–26 May 1983; pp. 131–134.
15. Lizzi, F.; Viggiani, C.; Vinale, F. Some experience with pre-loading cells at the base of large diameter bored piles. In Proceedings of the 7th Asian Regional Conference on Soil Mechanics and Foundation Engineering, Haifa, Israel, 14–19 August 1983.
16. Stocker, M.F. The influence of post grouting on the load bearing capacity of bored piles. In Proceedings of the 8th European Conference on Soil Mechanics and Foundations Engineering, Helsinki, Finland, 23–26 May 1983; pp. 167–170.
17. Gouvenot, D.; Gabiax, F.D. A new foundation technique using piles Sealed by Concrete Under High Pressure. In Proceedings of the 7th Auunal Offshore Technical Conference, Huston, TX, USA, 5–8 May 1975.
18. Thiyyakkandi, S.; McVay, M.; Bloomquist, D.; Lai, P. Measured and predicted response of a new jetted and grouted precast pile with membranes in cohesionless soils. *J. Geotech. Geoenviron. Eng.* **2013**, *139*, 1334–1345. [CrossRef]
19. Wan, Z.; Liu, H.; Zhou, F.; Dai, G. Axial Bearing Mechanism of Post-Grouted Piles in Calcareous Sand. *Appl. Sci.* **2022**, *12*, 2731. [CrossRef]
20. Bayesteh, H.; Fakharnia, M. Numerical simulation of load tests on hollow-bar micropiles considering grouting method. *Proc. Inst. Civ. Eng. Geotech. Eng.* **2022**, *175*, 15–30. [CrossRef]
21. Youn, H.; Tonon, F. Numerical analysis on post-grouted drilled shafts: A case study at the Brazo River Bridge, TX. *Comput. Geotech.* **2010**, *37*, 456–465. [CrossRef]
22. Amadei, B.; Savage, W.Z. An analytical solution for transient flow of Bingham viscoplastic materials in rock fractures. *Int. J. Rock Mech. Min. Sci.* **2001**, *38*, 285–296. [CrossRef]
23. Bouchelaghem, F.; Almosni, A. Experimental determination of the longitudinal dispersivity during the injection of a micro-cement grout in a one-dimensional soil column. *Transp. Porous Media* **2003**, *52*, 67–94. [CrossRef]
24. Jafarpour, P.; Moayed, R.Z.; Kordnaeij, A. Behavior of zeolite-cement grouted sand under triaxial compression test. *J. Rock Mech. Geotech. Eng.* **2020**, *12*, 149–159. [CrossRef]
25. Maghous, S.; Saada, Z.; Dormieux, L.; Canou, J.; Dupla, J.C. A model for in situ grouting with account for particle filtration. *Comput. Geotech.* **2007**, *34*, 164–174. [CrossRef]
26. Saada, Z.; Canou, J.; Dormieux, L.; Dupla, J.C. Evaluation of elementary filtration properties of a cement grout injected in a sand. *Can. Geotech. J.* **2006**, *43*, 1273–1289. [CrossRef]

27. Saada, Z.; Canou, J.; Dormieux, L.; Dupla, J.C.; Maghous, S. Modelling of cement suspension flow in granular porous media. *Int. J. Numer. Anal. Methods Geomech.* **2005**, *29*, 691–711. [CrossRef]
28. Mozumder, R.A.; Laskar, A.I.; Hussain, M. Penetrability prediction of microfine cement grout in granular soil using Artificial Intelligence techniques. *Tunn. Undergr. Space Technol.* **2018**, *72*, 131–144. [CrossRef]
29. Shrivastava, N.; Zen, K. An experimental study of compaction grouting on its densification and confining effects. *Geotech. Geol. Eng.* **2018**, *36*, 983–993. [CrossRef]
30. Huang, Y.H.; Zhuang, X.X.; Wang, P.P.; Zong, Z.L. Axial behavior of pressure grouted helical piles installed in marine soft clay based on full-scale field tests. *Geotech. Geol. Eng.* **2022**, *40*, 5799–5812. [CrossRef]
31. Lai, V.Q.; Keawsawasvong, S.; Shiau, J. Analysis of shaft-grouted piles using load-transfer method. *Int. J. Geosynth. Ground Eng.* **2022**, *8*, 10. [CrossRef]
32. Liu, S.W.; Zhang, Q.Q.; Li, H.T.; Yu, X.T.; Liu, G.H.; Cui, W. An analysis method for the response of combined side-and-tip grouting pile. *Acta Geotech.* **2023**, *15*, 3715–3729. [CrossRef]
33. Zhao, C.F.; Wu, Y.; Zhao, C.; Wang, Y. Load-displacement relationship of single piles in clay considering different tip grouting volumes and grouting returned heights. *Int. J. Geomech.* **2020**, *20*, 04019158. [CrossRef]
34. Chang, M.F.; Zhu, H. Construction effect on load transfer along bored piles. *J. Geotech. Geoenviron. Eng.* **2004**, *130*, 426–437. [CrossRef]
35. Fei, Y.; Yasufuku, N.; Zhao, C.F.; Zhao, C.; Xu, K. Shear behaviour of sand-concrete interface with side post-grouting considering the unloading effect. *Soils Found.* **2020**, *60*, 1440–1449. [CrossRef]
36. Kulhawy, F.H.; Kozera, D.W.; Withiam, J.L. Uplift testing of model drilled shafts in sand. *J. Geotech. Eng. Div. Asc.* **1979**, *105*, 31–47. [CrossRef]
37. Khalid, U.; Ye, G.L.; Yadav, S.K.; Zhou, A.; Gu, L. Consolidation Pressure Consequences on the Soil Structure of Artificial Structured Marine Clay: Macro and Micro Evaluation. *Geotech. Geol. Eng.* **2021**, *39*, 247–263. [CrossRef]
38. Khalid, U.; Rehman, Z.; Mujtaba, H.; Farooq, K. 3D response surface modeling based in-situ assessment of physico-mechanical characteristics of alluvial soils using dynamic cone penetrometer. *Transp. Geotech.* **2022**, *36*, 100781. [CrossRef]

Disclaimer/Publisher's Note: The statements, opinions and data contained in all publications are solely those of the individual author(s) and contributor(s) and not of MDPI and/or the editor(s). MDPI and/or the editor(s) disclaim responsibility for any injury to people or property resulting from any ideas, methods, instructions or products referred to in the content.